

LETTER

Manipulation of the terahertz leaky wave by metal–dielectric–metal metasurface

To cite this article: Qingqing Cheng *et al* 2019 *Appl. Phys. Express* **12** 072008

View the [article online](#) for updates and enhancements.



Manipulation of the terahertz leaky wave by metal–dielectric–metal metasurface

Qingqing Cheng^{1*}, Chaoshi Zhang¹, Dong Yu¹, Lin Chen¹, Jingya Xie¹, Xiaofei Zang¹, Alexander Shkurinov², Yiming Zhu^{1*}, and Songlin Zhuang¹

¹Terahertz Technology Innovation Research Institute, Terahertz Spectrum and Imaging Technology Cooperative Innovation Center, Shanghai Key Lab of Modern Optical System, University of Shanghai for Science and Technology, Shanghai 200093, People's Republic of China

²Faculty of Physics, Lomonosov Moscow State University, 119991 Leninskie gori 1/2, Moscow, Russia

*E-mail: qqcheng@usst.edu.cn; ymzhu@usst.edu.cn

Received March 26, 2019; revised May 1, 2019; accepted June 7, 2019; published online June 20, 2019

We experimentally demonstrated the properties of leaky waves generated inside the air gap between a high-index prism and a metal–dielectric–metal metasurface can be strongly engineered by the geometrical parameters of the metasurface. In particular, we further identified that the excited leaky waves undergo a transition from an over-coupled state to an under-coupled state along with the variation of structure parameters, manifest in their strongly engineered optical responses. These experimental findings can be well explained by the coupled-mode theory, and may have potential implementation in sensitive sensors and detections based on leaky waves. © 2019 The Japan Society of Applied Physics

Leaky waves are ubiquitous and excited at the interfaces of hybrid waveguides,^{1,2)} dielectric waveguides³⁾ or surface plasmon polaritons (SPP) waveguides.^{4–8)} Meanwhile, they have been successfully applied to demonstrate several intriguing phenomena, such as Cherenkov radiations,⁹⁾ Wood's anomalies,¹⁰⁾ extraordinary optical transmissions,¹¹⁾ etc. Furthermore, leaky waves induced from total internal reflections have also been widely used in the scientific areas of substance detections,¹²⁾ waveguide coupling,¹³⁾ and antenna radiations.^{14,15)} Especially, many functional devices have been developed based on the leaky waves in the terahertz region, for example, antennas,¹⁴⁾ near-field probes,¹⁶⁾ leaky-lenses¹⁷⁾ and frequency-division multiplexers.¹⁴⁾ However, there is still a lack of effective near-field engineering method on leaky waves due to the short decay length.

Recently, diversified wave manipulation methods have emerged in the terahertz¹⁸⁾ and microwave range^{19,20)} by operating with metal–dielectric–metal (MDM) metasurfaces. The principle is based on the magnetic resonance enhanced by the antisymmetric oscillation mode of two coupled layers. MDM metasurfaces are widely applied for engineering polarizations,²¹⁾ phases,^{22,23)} and amplitudes of incident light.^{22,24)} Researchers have also developed other various MDM metasurface-based optical devices including flat lenses,²⁵⁾ beam deflectors,²⁶⁾ wave plates,²⁷⁾ vortex generators^{28,29)} and holograms.^{30,31)} Most of the demonstrated MDM metasurfaces are widely applied in the engineering of the free space light,^{32–37)} but there have been few reports on leaky waves.

In this work, an MDM metasurface is used to engineer the optical response of terahertz leaky waves. Here, we reveal that the capping periodic slit in MDM metasurface has a critical transition width. When the slit width is less than the critical width, the optical response is over-coupled, while the optical response is under-coupled in the opposite case. These two optical responses in the MDM metasurface are clearly described by the coupled-mode theory,³⁸⁾ which depend on the relative ratio between the radiation loss and the absorption loss in the resonator (MDM metasurface structure).^{18,22)} These two radiation loss rates are the intrinsic loss rate of the resonance due to materials absorption γ_{abs} and the energy external leakage rate γ_{rad} radiated from the resonator, respectively. In particular, the transition of the optical responses is experimentally demonstrated via tuning the

parameters of the metasurface, or incident angle of the beam which is equivalent to the angle of the prism. In comparison with traditional bulky configurations for leaky waves, the engineering of leaky waves in the near-field region by the thinner MDM metasurface is more efficient and practicable for potential applications of biomolecule sensors.

The MDM metasurface is depicted in Fig. 1(a), which consists of a metal grating on the top and a metal plate at the bottom, with a sandwich layer of silicon. The top metallic layer consists of periodic air slits with periodic spacing of d and slit width of a . The thicknesses of the metallic and the dielectric layers are t and h , respectively. The terahertz waves are incident horizontally from left side of the Teflon prism, for which the wedge angle is designed to meet the total internal reflection and thus the leaky wave is excited at the interface between the metal grating and the air. The bottom metallic film prohibits any transmission through the MDM device so that only the reflection of the device needs to be taken into account. Moreover, near-field coupling between two metallic layers can form a series of resonances at frequencies dictated by the geometrical details, each with induced currents flowing in opposite directions on the two metallic layers. When these resonances are comparably separated in the frequency domain for which the peak width of each mode is much less than the inter-mode frequency difference, the device can be well described by a one-port single-mode resonator model at the specific resonance frequency of ω_0 . To understand the nature of the MDM device, we depict a conceptual model in Fig. 1(b). This model assumes that an incident light wave can be reflected from the metasurface by flowing through two channels: the intrinsic loss rate γ_{abs} and the energy external leakage rate γ_{rad} .

When the transverse component of the wave vector of the incident light matches the propagation constant of Spoof SPP (eigenmode), the incident E -field with x -polarized can be resonantly coupled to the metasurface. The incident wave vector exists in the range $0 < k_x < n\omega/c$, where n is the refractive index of the prism. The impedance matching condition occurs between the incident field and the eigenmode of the MDM metasurface, hence resulting in an absorption valley in the spectra of the reflection amplitude. The coupled interaction can be characterized by the spectra of reflection amplitude and phase as functions of slit widths,

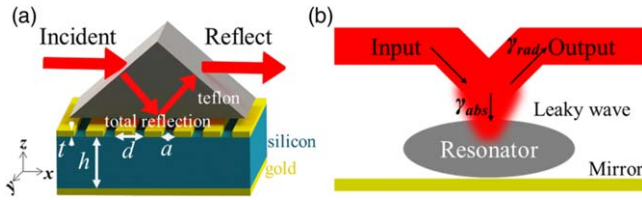


Fig. 1. (Color online) Design of a metal–dielectric–metal (MDM) metasurface. (a) Schematic of terahertz leaky wave engineered by the MDM metasurface. Terahertz wave is incident from the left side and reflected by the Teflon prism. (b) Intuitive model for the incident light can be directly reflected or follow a resonant pathway through the single-port resonator model in CMT.

dielectric layer thicknesses and wedge angles. Using Coupled-Mode-Theory, the following expression for the reflection coefficient can be derived:

$$r_{\text{tot}} = \frac{(\gamma_{\text{rad}} - \gamma_{\text{abs}}) - i(\omega - \omega_0)}{(\gamma_{\text{rad}} + \gamma_{\text{abs}}) + i(\omega - \omega_0)}. \quad (1)$$

Here, ω_0 is the resonance angular frequency. From Eq. (1), the total reflection phase varies continuously from -180° to 180° in the under-coupled region ($\gamma_{\text{abs}} > \gamma_{\text{rad}}$), and less than 180° in the over-coupled region ($\gamma_{\text{abs}} < \gamma_{\text{rad}}$) at the given resonance frequency of ω_0 . Based on the above analysis and Eq. (1), the total reflectivity of the leaky wave engineered by MDM is fully determined by γ_{abs} and γ_{rad} . Derived from mode expansion theory^{18,20} by approximation conditions ($a \ll \lambda, d \ll \lambda, h < \lambda$), we conclude that both γ_{rad} and γ_{abs} are related to the thickness of the spacer, and γ_{abs} is also strongly related to the slit width.²⁰ From these two relations, both γ values can be easily tuned by well-designed device parameters.

In order to study the spectra of the reflection amplitude and phase of the devices, numerical simulations are employed. We assume the relative permittivity of the Au layer is $\epsilon_{\text{Au}} = \epsilon_{\text{inf}} - \omega_p^2 / (\omega^2 - i\omega\gamma)$, where $\epsilon_{\text{inf}} = 1.53$, $\omega_p = 2\pi \times 2.069 \times 10^{15}$ Hz and $\gamma = 2\pi \times 1.764 \times 10^{13}$ Hz. The refractive index of the silicon layer is $n_{\text{si}} = 3.5$ with a negligible imaginary part of the refractive index, and the slit width varies from 10 to 100 μm . The simulation results indicate there are two absorption peaks corresponding to the resonances in the device, as shown in the Fig. 2(a). Both resonances show blue shifts when the slit width increases: the low resonant frequency around $\omega_0 = 0.1$ THz varies from 0.085 to 0.132 THz, and the high resonant frequency at

$\omega_0 = 0.3$ THz slowly changes from 0.31 to 0.38 THz. As the spectra of the reflection amplitude of $|r|^2$ is not enough to distinguish the difference between the electromagnetic responses of the two resonance frequencies, it is necessary to consider the phase transitions $\Delta\phi$ of the spectra of the reflection shown in Fig. 2(b). Interestingly, the slit has a critical transition width at $a = 23.5 \mu\text{m}$. When the slit width is less than 23.5 μm , the phase transitions at the high resonance frequency can be less than 180° . Our results clearly show that whether the phase transition at the high-frequency resonance point exceeds 180° or not depends on the slit width of the device.

To better understand the optical response around the critical transition width, two slit widths of $a_1 = 20 \mu\text{m}$ and $a_2 = 40 \mu\text{m}$ are theoretically selected to retrieve the γ_{abs} and the γ_{rad} value. Full wave simulations were then first performed to study their field distributions [Fig. 2(c) for the two slit widths of $a_1 = 20 \mu\text{m}$ and $a_2 = 40 \mu\text{m}$]. The field-distributed simulation of $a_1 = 20 \mu\text{m}$ depicted in Fig. 2(c) stores more electromagnetic field energy in the air domain, indicating that the value of $\gamma_{\text{rad}} = 33.2$ is larger than the value of $\gamma_{\text{abs}} = 14$, which is in good agreement with the value of $\gamma_{\text{rad}} = 33.4$ and the value of $\gamma_{\text{abs}} = 14.4$ retrieved from the analytical method. From the simulation results with the metal slit width $a_2 = 40 \mu\text{m}$, as shown in Fig. 2(c), we can see that more electromagnetic field energy is stored in the silicon layer compared with the former case. The value of $\gamma_{\text{abs}} = 46.4$ is larger than the value of $\gamma_{\text{rad}} = 20.7$, which also matches the analytic results. The distinct behaviors in the spectra of the reflection phase of different slit widths indicate a phase transition from the over-coupled to the under-coupled resonance, as the slit width increases from 20 to 40 μm . And in particular, the process can be undergone a fully absorbed state that is extremely sensitive to perturbations.

These above-mentioned predictions are then consistently verified by both experiments and simulations. We fabricate a series of MDM device with different slit widths. The fabrication follows the standard optical lithography procedures. First, in order to improve the adhesion of the gold film to the silicon wafer, hexamethyldisilazane (HDMS) is spin-coated on the surface of the silicon wafer. A one-dimensional grating structure is prepared through a non-mask lithography machine (UPG501). After the lift-off process, the MDM devices are prepared finally, and the schematic diagram of the MDM is presented in Fig. 1(a), wherein the metal slit width is

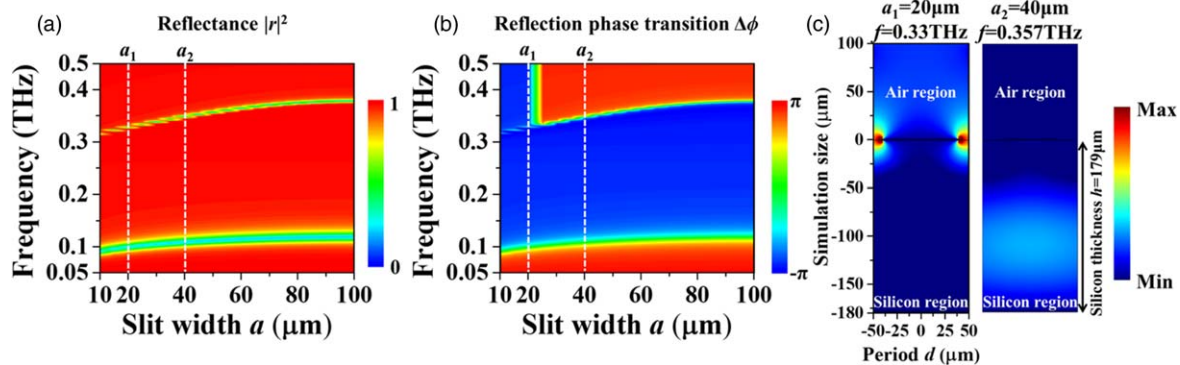


Fig. 2. (Color online) The spectrum of the reflection amplitude and phase. (a) The MDM structure with different slit widths from 10 to 100 μm . (b) Phase transition $\Delta\phi$ of the reflection spectra of the MDM metasurface. (c) The over-coupled state with slit width $a_1 = 20 \mu\text{m}$ and under-coupled state with slit width $a_2 = 40 \mu\text{m}$. Geometric parameters of the MDM are $d = 100 \mu\text{m}$, $h = 179 \mu\text{m}$, and all metallic films have thicknesses of $t = 60$ nm.

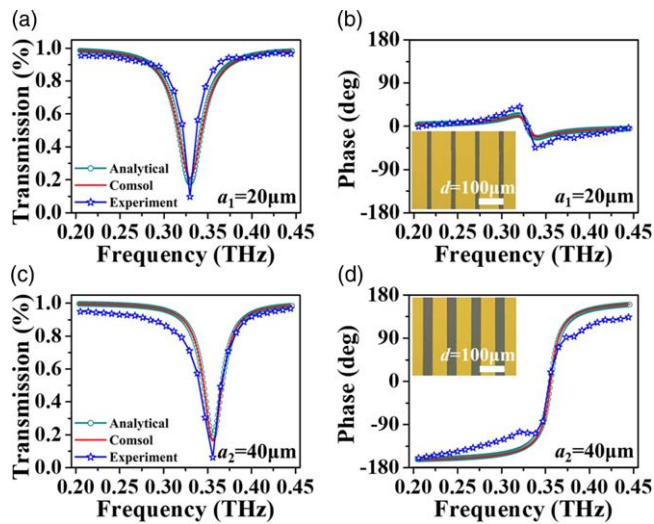


Fig. 3. (Color online) Comparison between the analytical, the numerically simulated and the experimental results. Reflectance of the leaky waves with $a_1 = 20 \mu\text{m}$ (a) and $a_2 = 40 \mu\text{m}$ (c). Phase transitions with $a_1 = 20 \mu\text{m}$ (b) and $a_2 = 40 \mu\text{m}$ (d), the optical responses are over-coupled with $a_1 = 20 \mu\text{m}$ and under-coupled with $a_2 = 40 \mu\text{m}$. Insets show the fabricated samples with the white scale bar $100 \mu\text{m}$.

$a_1 = 20 \mu\text{m}$ and $a_2 = 40 \mu\text{m}$, and the grating periodicity is $d = 100 \mu\text{m}$. The thicknesses of the metallic and spacer layer are $t = 60 \text{ nm}$ and $h = 179 \mu\text{m}$, respectively. Optical images of two typical samples are shown in the insets of Figs. 3(b) and 3(d). In a dry air environment, we use the THz time-domain spectroscopy to measure the spectra of the reflection amplitude and phase of the reflected leaky wave, wherein the signal of the metal plate is a reference signal. The measured time domain signal is then Fourier transformed to the spectral domain, and its amplitude and phase information are derived with the normalization to the reference signal. $r(\omega) = r_s(\omega)/r_r(\omega)$, where $r_s(\omega)$ is the reflected signal and $r_r(\omega)$ is the reference signal. The amplitude and the phase transition of the MDM device are experimentally measured with the slit width of $a_1 = 20 \mu\text{m}$ as shown in Figs. 3(a) and 3(b), respectively. The transverse component of the leaky wave vector matches the wave vector of the eigenmode in the MDM device, which means that the incident electromagnetic field is coupled to the eigenmode such that an absorption valley occurs in the reflection spectra, as shown in Fig. 3(a). Furthermore, in Fig. 3(b), the resonance frequency of 0.3 THz exhibits a phase transition of less than 180° in the experiment, that is, an over-coupled state with the value of $\gamma_{\text{abs}} = 14.3$ and $\gamma_{\text{rad}} = 33.3$. The measured spectra are in good agreement with

the finite-difference time domain simulations for the realistic structures.

Similarly, a reflection spectra (blue symbol) and a phase transition (blue symbol) with a slit width of $a_2 = 40 \mu\text{m}$ were experimentally measured as shown in Figs. 3(c) and 3(d). The resonance frequency blue-shifted to 0.357 THz compared with the case when the slit width $a_1 = 20 \mu\text{m}$. In the interval range from 0.25 to 0.45 THz, the phase transition of the reflection spectra can cover 360° , which is in an under-coupled state. Finally, the functionality can be realized by tuning the duty ratio of the periodic slit width of the MDM device. We quantitatively retrieve the values of γ_{abs} and γ_{rad} by fitting the measured and the simulated spectra of different slit widths to Eq. (1), and get the results that the value of γ_{abs} is 46.6 which is larger than the value of $\gamma_{\text{rad}} = 20.8$. Such retrieved values are in good agreement with the numerically simulated and the analytical results.

To explicitly study the mechanism of the optical response incurred by the MDM device at these two resonance frequencies with other parameters, we first investigate whether the dielectric layer thickness influences the optical response of the leaky wave. As shown in Fig. 4(a), the phase transition of the optical response at the high frequency is verified by the Smith curve of the reflection coefficient. When h becomes thinner ($h_1 = 169 \mu\text{m}$ and $h_2 = 179 \mu\text{m}$), the Smith curve (black and red curves) only passes through the second and the third quadrants, with the phase of the reflection varying from 90° to 270° in the over-coupled state. With the increase of h ($h_3 = 189 \mu\text{m}$ and $h_4 = 199 \mu\text{m}$), the Smith curve (the blue and the green curves) covers four quadrants. And the achieved reflection phase can cover from 0° to 360° in the under-coupled state. Therefore, the simulation shows that the optical response of the terahertz leaky wave in the MDM device can be engineered by changing the thickness of the dielectric layer. In addition, as shown in Fig. 4(b), when the layer thickness is fixed at $h = 179 \mu\text{m}$ and the slit width is $a = 20 \mu\text{m}$, the optical response at the resonance frequency of 0.1 THz is over-coupled. In this case, the optical response at the 0.3 THz resonance frequency is under-coupled, and there is a combination of the optical responses in the same device. On the other hand, when the thickness of the spacer changes to $h = 189 \mu\text{m}$ [see Fig. 4(c)], the optical response states at the resonance frequencies of 0.1 and 0.3 THz exhibit an under-coupled state with the slit width of $a = 40 \mu\text{m}$.

The influences of the wedge angle of the prism on the optical response at the resonance frequency are also

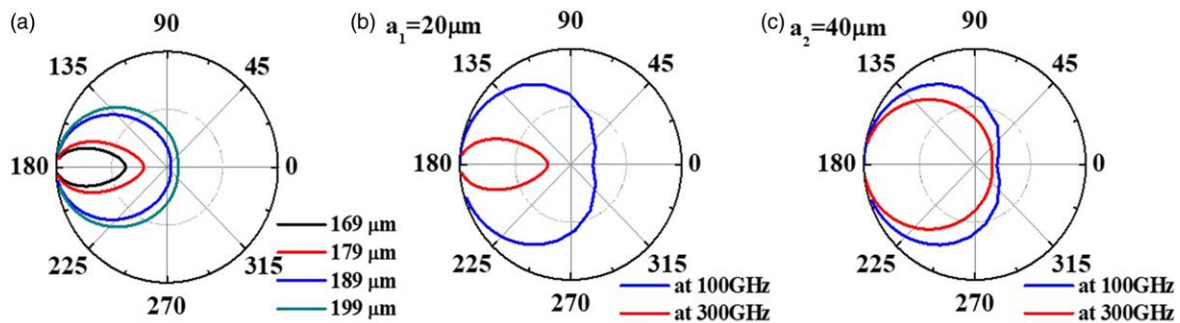


Fig. 4. (Color online) Simulation results with different thicknesses of the spacer. (a) Smith curves of the reflectance of the sample for different thicknesses of the spacer. (b) The slit width of $a = 20 \mu\text{m}$ and the layer thickness of $h = 179 \mu\text{m}$, the Smith curve for the frequency at 0.1 THz and 0.3 THz, respectively. (c) The slit width of $a = 40 \mu\text{m}$ and the layer thickness of $h = 189 \mu\text{m}$.

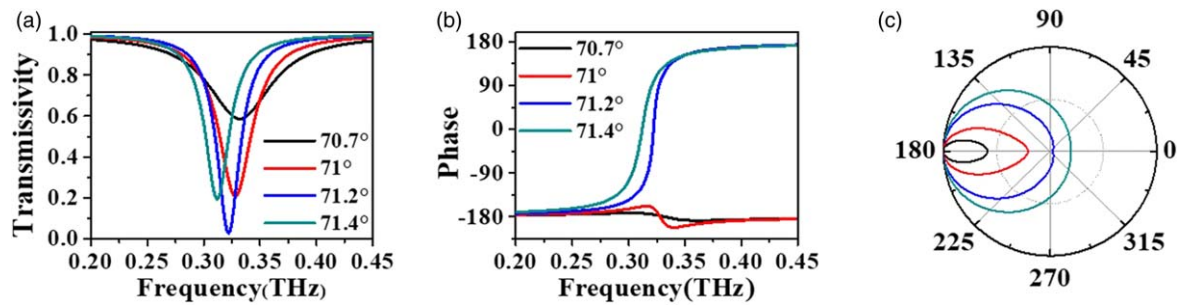


Fig. 5. (Color online) Simulation results with different wedge angles of the Teflon prism. (a) The reflectance with different wedge angles 70.7°, 71°, 71.2°, and 71.4°. (b) The phase transitions. (c) The Smith curve.

investigated. It is intuitive to realize that the change of the wedge angle of the prism affects the horizontal wave vector of the leaky wave, which matches the wave vector of the eigenmode in the MDM device. The eigenmode wave vectors at different frequencies are different, so the horizontal wave vector corresponding to the wedge angle can select a specific frequency and generate a resonance. In the simulation, when the wedge angles of the prism are 70.7°, 71°, 71.2°, and 71.4°, there are similar resonance frequencies at the range from 0.2 to 0.45 THz, as shown in Fig. 5(a). In particular, the optical response appears to be over-coupled when the wedge angles are 70.7° and 71°, whereas the optical response appears to be under-coupled when the angles are 71.2° and 71.4°, as shown in Fig. 5(b). In addition, this also coincides with the Smith curve from the reflection line in Fig. 5(c).

In conclusion, we have demonstrated theoretically and experimentally the existence of critical transition width for distinguishing the under-coupled and over-coupled optical responses during the engineering process of the terahertz leaky wave based on the MDM metasurface. The radiation rate γ_{rad} and the absorption rate γ_{abs} influence the impedance matching of the eigen-mode in the MDM metasurface and the terahertz leaky waves, which induce these two optical responses. It is demonstrated that the optical responses are strongly related to the slit width, the silicon thickness and the wedge angle. Furthermore, by carefully selecting the parameters such as slit widths and spacer thicknesses, the optical response has two states simultaneously. Our structure has the ability to be directly integrated into nano-photonics devices owing to its ultrathin property. Its simple geometry is very amenable to advanced large area nanofabrication techniques and thus is beneficial for applications of biomolecular detections and characterizations of material refractive index.

Acknowledgments This work was supported in part by the Major National Development Project of Scientific Instrument and Equipment (2016YFF0100503), in part by the National Natural Science Foundation of China (Nos. 11874266, 11604208, 61705131, 61722111), the 111 Project (D18014), the International Joint Lab Program supported by Science and Technology Commission Shanghai Municipality (17590750300), Shanghai Science and Technology Committee (Nos. 16ZR1445600, 16ZR1445500), Shanghai Chenguang Program (17CG49).

- 1) R. F. Oulton, V. J. Sorger, D. A. Genov, D. F. P. Pile, and X. Zhang, *Nat. Photonics* **2**, 496 (2008).
- 2) Q. Q. Cheng, T. Li, R. Y. Guo, L. Li, S. M. Wang, and S. N. Zhu, *Appl. Phys. Lett.* **101**, 171116 (2012).
- 3) S. Jahani and Z. Jacob, *Nat. Nanotechnol.* **11**, 23 (2016).
- 4) S. I. Bozhevolnyi, V. S. Volkov, E. Devaux, J.-Y. Laluet, and T. W. Ebbesen, *Nature* **440**, 508 (2006).

- 5) H. F. Ma, X. P. Shen, Q. Cheng, W. X. Jiang, and T. J. Cui, *Laser Photonics Rev.* **8**, 146 (2014).
- 6) Q. Q. Cheng, T. Chen, D. Yu, Y. J. Liao, J. Y. Xie, X. F. Zang, X. P. Shen, and Y. M. Pan, *Opt. Express* **26**, 31636 (2018).
- 7) Q. Q. Cheng, Y. M. Pan, H. Q. Wang, C. S. Zhang, D. Yu, A. Gover, H. J. Zhang, T. Li, L. Zhou, and S. N. Zhu, *Phys. Rev. Lett.* **122**, 173901 (2019).
- 8) S. P. Zhang, H. Wei, K. Bao, U. Håkanson, N. J. Halas, P. Nordlander, and H. X. Xu, *Phys. Rev. Lett.* **107**, 096801 (2011).
- 9) B. F. Monticone and A. Alu, *Proc. IEEE* **103**, 793 (2015).
- 10) Hessel and A. A. Oliner, *Appl. Opt.* **4**, 1275 (1965).
- 11) Z. Liu, P. W. C. Hon, A. A. Tavallaei, T. Itoh, and B. S. Williams, *Appl. Phys. Lett.* **100**, 074510 (2012).
- 12) B. Zheng, H. Q. Zhao, B. Cerjan, S. Yazdi, E. Ringe, P. Nordlander, and N. J. Halas, *Appl. Phys. Lett.* **113**, 101105 (2018).
- 13) Q. Q. Cheng, Y. Pan, Q. Wang, T. Li, and S. N. Zhu, *Laser Photonics Rev.* **9**, 392 (2015).
- 14) N. J. Karl, R. W. McKinney, Y. Monnai, R. Mendis, and D. M. Mittleman, *Nat. Photonics* **9**, 717 (2015).
- 15) D. A. Chu, P. W. C. Hon, T. Itoh, and B. S. Williams, *J. Appl. Phys.* **120**, 013103 (2016).
- 16) W. Bao, M. Staffaroni, J. Bokor, M. B. Salmeron, E. Yablonovitch, S. Cabrini, A. W. Bargioni, and P. J. Schuck, *Opt. Express* **21**, 8166 (2013).
- 17) A. J. Martínez-Ros, J. L. Gómez-Tornero, F. J. Clemente-Fernández, and J. Monzó-Cabrera, *IEEE Trans. Antennas Propag.* **61**, 2981 (2013).
- 18) C. Qu et al., *Phys. Rev. Lett.* **115**, 235503 (2015).
- 19) W. J. Sun, Q. He, S. L. Sun, and L. Zhou, *Light Sci. Appl.* **5**, 16003 (2016).
- 20) S. Ma, S. Xiao, and L. Zhou, *Phys. Rev. B* **93**, 045305 (2016).
- 21) Y. Lin, L. Wang, J. Gao, Y. Lu, S. Jiang, and W. Zeng, *Appl. Phys. Express* **10**, 032001 (2017).
- 22) J. Park, J. H. Kang, S. J. Kim, X. Liu, and M. L. Brongersma, *Nano Lett.* **17**, 407 (2017).
- 23) Y. W. Huang, H. W. H. Lee, R. Sokhoyan, R. A. Pala, K. Thyagarajan, S. Han, D. P. Tsai, and H. A. Atwater, *Nano Lett.* **16**, 5319 (2016).
- 24) Z. Q. Miao, Q. Wu, X. Li, Q. He, K. Ding, Z. H. An, Y. B. Zhang, and L. Zhou, *Phys. Rev. X* **5**, 041027 (2015).
- 25) M. G. Pors, R. L. Nielsen, Eriksen, and S. I. Bozhevolnyi, *Nano Lett.* **13**, 829 (2013).
- 26) J. Neu, R. Beigang, and M. Rahm, *Appl. Phys. Lett.* **103**, 041109 (2013).
- 27) N. F. Yu, F. Aieta, P. Genevet, M. A. Kats, Z. Gaburro, and F. Capasso, *Nano Lett.* **12**, 6328 (2012).
- 28) E. Karimi, S. A. Schulz, I. D. Leon, and R. W. Boyd, *Light Sci. Appl.* **3**, e167 (2014).
- 29) Y. M. Yang, W. Y. Wang, P. Moitra, I. I. Kravchenko, D. P. Briggs, and J. Valentine, *Nano Lett.* **14**, 1394 (2014).
- 30) X. Ni, A. V. Kildishev, and V. M. Shalae, *Nat. Commun.* **4**, 2807 (2013).
- 31) L. Q. Cong, P. Pitchappa, Y. Wu, L. Ke, C. K. Lee, N. Singh, H. Yang, and R. Singh, *Adv. Opt. Mater.* **5**, 1600716 (2017).
- 32) G. X. Zheng, H. Mühlenbernd, M. Kenney, G. X. Li, T. Zentgraf, and S. Zhang, *Nat. Nanotechnol.* **10**, 308 (2015).
- 33) S. M. Kamali, E. Arbabi, A. Arbabi, and A. A. Faraon, *Nanophotonics* **7**, 1041 (2018).
- 34) Q. He, S. L. Sun, S. Y. Xiao, and L. Zhou, *Adv. Opt. Mater.* **6**, 1800415 (2018).
- 35) P. Genevet, F. Capasso, F. Aieta, M. Khorasaninejad, and R. Devlin, *Optica* **4**, 139 (2017).
- 36) H.-H. Hsiao, C. H. Chu, and D. P. Tsai, *Small Methods* **1**, 1600064 (2017).
- 37) V. C. Su, C. H. Chu, G. Sun, and D. P. Tsai, *Opt. Express* **26**, 13148 (2018).
- 38) S. H. Fan, W. Suh, and J. D. Joannopoulos, *J. Opt. Soc. Am. A* **20**, 569 (2003).